Article

Not peer-reviewed version

Analysis of Process Parameters and Particle Characteristics During Biomass Fast Pyrolysis: Effect on Biomass Conversion and Main Products Yields

Mario A. Sánchez * , Juan C. Maya , Nevis A. Ruiz-Márquez , Fabian Luna

Posted Date: 22 April 2026

doi: 10.20944/preprints202604.1537.v1

Keywords: biomass pyrolysis; fast pyrolysis; single particle model; bio-oil; biochar

 doi:10.20944/preprints202604.1537.v1

Article

Analysis of Process Parameters and Particle Characteristics During Biomass Fast Pyrolysis: Effect on Biomass Conversion and Main Products Yields

Mario A. Sánchez [1,*], Juan C. Maya [2], Nevis A. Ruiz-Márquez [3] and Fabian Luna [1]

[1] Escuela de Ingeniería y Ciencias Básicas, Universidad EIA, Envigado 055428, Colombia
[2] Grupo de Investigación TAYEA, Departamento de Procesos y Energía, Facultad de Minas, Universidad Nacional de Colombia-Sede Medellín, Medellín 050034, Colombia
[3] Grupo de investigación CBATA, Tecnológico de Antioquia Institución Universitaria, Medellín 050034, Colombia
* Correspondence: mario.sanchez@eia.edu.co

Abstract

A computational model of anisotropic biomass particle pyrolysis was used to study the influence of particle properties and process conditions. The model couples multicomponent CRECK kinetics with intraparticle heat and mass transport. Particle size and lignocellulosic composition significantly affect conversion time and product yields; aspect ratio was also found to be important for larger-diameter particles. Larger particles (8 mm diameter, 4:1 aspect ratio) showed conversion times more than twice those of 3 mm particles, and char yield increased from about 16% to 23% when comparing small and large particles. Lignin-rich materials (e.g., palm shell) produced higher char and lower volatile yields than cellulose-rich biomass (wood, sugarcane bagasse); for 3 mm particles, char changed from 16% (oak) to 23% (palm shell). Higher reactor temperatures and heating rates substantially shortened particle conversion time—by up to 75%—and noticeably affected product yields. Analysis of the Biot and Pyrolysis numbers indicates millimeter-scale particles operate in a transition regime where internal conduction, external convection, and chemical kinetics occur on comparable timescales, so models must include these phenomena to accurately predict conversion times and final yields for reactor design and optimization.

Keywords: biomass pyrolysis; fast pyrolysis; single particle model; bio-oil; biochar

1. Introduction

Fast pyrolysis of lignocellulosic biomass has attracted significant interest as a thermochemical conversion pathway for producing renewable fuels and chemicals. In this process, biomass particles are rapidly heated in an inert atmosphere, typically at temperatures between 450 and 600 °C, yielding a liquid fraction (bio-oil), non-condensable gases, and a solid residue (char). The primary product of interest is the liquid fraction, whose yields under optimized conditions generally range from 50 to 70 wt.% Fast pyrolysis has emerged as a promising technology within the bioeconomy due to the wide availability of biomass feedstocks and its near carbon-neutrality .

At the single-particle scale, fast pyrolysis is governed by four principal intraparticle phenomena that occur simultaneously and are strongly coupled: heat transfer, mass transfer, chemical reactions, and phase changes [3]. The complexity of their interaction has driven the development of progressively more detailed computational models. Early approaches relied on simplified one-dimensional heat transfer descriptions and lumped kinetic schemes, whereas more recent studies incorporate two-dimensional anisotropic transport, multi-component reaction mechanisms, particle shrinkage, and intraparticle phase changes such as moisture evaporation and liquid intermediate formation [2]. The use of dimensionless numbers—namely the Biot number (Bi) and the pyrolysis

 doi:10.20944/preprints202604.1537.v1

numbers (Py_1, Py_2), as introduced by Pyle and Zaror [4] — provides a well-established framework to identify the dominant mechanisms governing conversion under given particle and operating conditions. When Bi > 1 and Py < 1, the process is typically classified within the conduction-controlled regime, where intraparticle heat transfer limitations dominate over external convection [3]. Under these conditions—which are representative of the millimeter-scale particles considered in this work—significant temperature and concentration gradients develop inside the particle, making spatially resolved models essential for accurate prediction.

Several single-particle models for biomass fast pyrolysis incorporating heat and mass transport have been proposed . While more recent approaches include both diffusive and convective transport, particle shrinkage, and moisture evaporation, only a limited number simultaneously accounting for particle shape and anisotropy . Earlier two-dimensional models, such as those by Di Blasi , Blondeau and Jeanmart , and Gentile et al. , either neglected the liquid intermediate phase, relied on global lumped reaction schemes, or did not consider conversion-dependent anisotropy. Sánchez et al. addressed these limitations by coupling two-dimensional anisotropic heat and mass transport with the CRECK kinetic scheme proposed by Debiagi et al. , incorporating key effects such as particle shrinkage, intraparticle flow, and a liquid intermediate phase, and validating the model against single-particle experiments for oak and birchwood . More recently, Crowley et al. extended this framework to pelletized feedstocks, combining experiments, XCT characterization, and computational modeling, and demonstrated that capturing dynamically evolving anisotropic transport properties is essential to reproduce experimental conversion behavior, while employing Biot and pyrolysis numbers to characterize the governing heat transfer regime .

Despite significant advances in single-particle modeling of biomass fast pyrolysis, a systematic assessment of how particle characteristics and operating conditions jointly affect intraparticle liquid intermediate dynamics and product yields—within validated anisotropic models with detailed kinetics—remains limited. Feedstock variability continues to hinder the scale-up of fast pyrolysis systems, as biomass exhibits a wide range of lignocellulosic compositions, particle sizes and shapes, and moisture contents, all of which strongly influence product distributions [2,17]. In addition, reactor operating conditions, particularly temperature and external heat transfer coefficients, span regimes that transition between different heat transfer limitations as described by the Biot and Pyrolysis numbers. In this context, a systematic parameter analysis within a physically consistent single-particle framework can provide quantitative insight for feedstock selection, preprocessing, and reactor design. The present work addresses this gap by performing a comprehensive parameter analysis of the model developed by Sánchez et al. [14], evaluating the effects of particle size, aspect ratio, and shrinkage; initial moisture content; lignocellulosic composition; reactor temperature; and convective heat transfer coefficient on biomass conversion, intraparticle liquid intermediate evolution, and product yields during fast pyrolysis.

2. Mathematical Model

2.1. Model Description

The single-particle model used in this work is described in detail by Sánchez et al. ; and only a summary is provided here. The conceptual basis of the model is illustrated in Figure 1, where the biomass particle is represented as a porous medium composed of a network of channels defined by solid cell walls. This representation enables a two-phase formulation consisting of a solid phase (cell walls), where heat conduction and heterogeneous reactions occur, and a fluid phase (pores), where gas-phase species are transported. In the axial direction, both convective and diffusive mechanisms contribute to heat and mass transport, whereas in the radial direction transport is primarily governed by thermal conduction through the solid matrix. This assumption is consistent with fast pyrolysis conditions, under which significant intraparticle temperature gradients develop. The governing equations and main model assumptions are summarized in Table 1.

 doi:10.20944/preprints202604.1537.v1

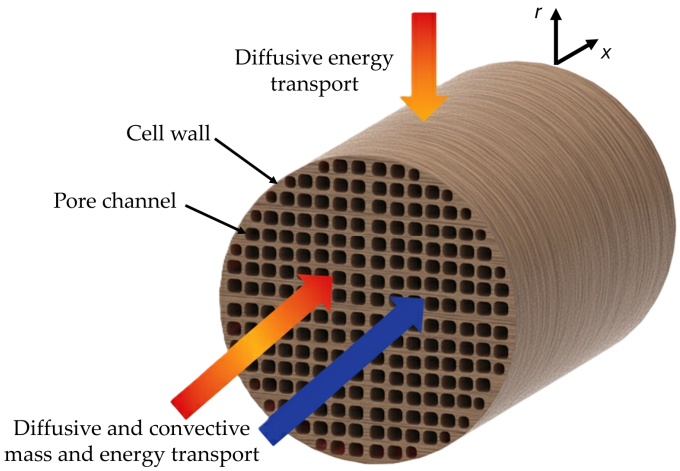

Figure 1. Schematic representation of transport mechanisms in a biomass particle under rapid pyrolysis conditions.

Table 1. Summary of main model considerations and governing equations.

Aspect	Consideration	Equation
Particle geometry	Porous anisotropic cylinder, radial and longitudinal shrinkage modeled as functions of average conversion.	$L_f = L_0(1 - \bar{\eta} \cdot s_{z,f})$ (1) $R_f = R_0(1 - \bar{\eta} \cdot s_{r,f})$ (2)
Reaction scheme	CRECK mechanism [15]: first-order Arrhenius kinetics	• 15 species • 7 liquid intermediate compounds • Lignin: hydrogen-rich lignin (LIG-H), oxygen-rich lignin (LIG-O), and carbon-rich lignin (LIG-C) • Active intermediates: CELLA, HCE1, HCE2, LIG-CC, LIG-OH, and LIG.
Solid/liquid phase mass balance	Biomass pseudo-components, metaplast and char	$\frac{\partial \rho_i^*}{\partial t} = \sum^{N_r} \dot{r}_{i,j}^{'''}(i = CELL,\ HCE,\ LIG-H,\ LIG-O,\ LIG-C,\ CELLA,\ HCE1,\ HCE2,\ LIG-OH,\ LIG,\ LIG-CC,\ char)$ (3)
Gas phase mass balance	Diffusive + convective transport in axial direction; diffusive only in radial direction:	$\frac{\partial \rho_i^*}{\partial t} = \frac{\partial}{\partial x}\left(\frac{D_{eff_G}}{\varepsilon_G}\frac{\partial \rho_i^*}{\partial x}\right) - \frac{\partial (v_G\ \rho_i^*)}{\partial x} + \sum \dot{r}_{i,j}^{'''}(i = GAS,\ VOL.,H_2O)$ (4)
Gas velocity	Darcy's Law	$v_G = -\frac{K_G}{\mu_G}\frac{\partial P}{\partial x}$ (5)

 doi:10.20944/preprints202604.1537.v1

Energy balance	Diffusive transport (axial + radial) + convective transport (axial) + heat of reactions	$\rho C_p \frac{\partial T}{\partial t} = \frac{\partial}{\partial x}\left(\lambda_{eff_x} \frac{\partial T}{\partial x}\right) + \frac{1}{r}\frac{\partial}{\partial r}\left(r\lambda_{eff_x} \frac{\partial T}{\partial r}\right) - \frac{\partial\left(v_G\, \rho_i^* C_{p,i} T\right)}{\partial x} + \sum \dot{r}_{i,j}^{'''} \Delta H_{R_j}$	(6)
Boundary conditions	Side boundary: convective heat and mass transfer	$\dot{N}_{x,i}^{''}\big\|_{x=L} = -D_{eff_G} \frac{\partial \rho_i^*}{\partial x} + v_G \rho_i^* = k_{m,i}\left(\rho_i^* - \rho_{i\,\infty}^*\right)$ $(i = GAS, VOL., H_2O)$	(7)
		$\dot{q}_{x,i}^{''}\big\|_{x=L} = -\lambda_{eff_x} \frac{\partial T}{\partial r} + v_G \rho_i^* C_{p,i} T = h(T_\infty - T_{x=L})$ $(i = GAS, VOL., H_2O)$	(8)
	Top boundary: convective heat and mass transfer	$\dot{N}_{x,i}^{''}\big\|_{r=R} = 0\ (i = GAS, VOL., H_2O)$	(9)
		$\dot{q}_{x,i}^{''}\big\|_{r=R} = -\lambda_{eff_r} \frac{\partial T}{\partial r} = h(T_\infty - T_{x=L})$ $(i = GAS, VOL., H_2O)$	(10)
	Symmetry boundaries: central axes	$\frac{\partial T}{\partial x}\Big\|_{x=0} = 0\ (i = b, c, L, G)$	(11)
		$\frac{\partial \rho_i^*}{\partial x}\Big\|_{x=0} = 0\ (i = b, c, L, G)$	(12)
		$\frac{\partial T}{\partial x}\Big\|_{r=0} = 0\ (i = b, c, L, G)$	(13)
		$\frac{\partial \rho_i^*}{\partial x}\Big\|_{r=0} = 0\ (i = b, c, L, G)$	(14)

The mass balances for the solid and liquid phases describe the evolution of biomass pseudo-components, liquid intermediates, and char through source terms derived from the CRECK kinetic mechanism. For the gas phase, transport includes both diffusion and convection along the axial direction, while radial transport is assumed to be purely diffusive, reflecting the strong anisotropy of wood permeability, where axial permeability can exceed radial permeability by several orders of magnitude . The energy balance incorporates conductive heat transfer in both spatial directions, together with axial convective transport associated with gas-phase motion and heat source terms from the CRECK scheme . These reactions shift from endothermic to exothermic behavior as conversion progresses toward char formation, thereby influencing intraparticle temperature gradients and overall conversion times . The effective thermal conductivity is calculated following Kollmann et al. , with modifications introduced by Sánchez et al. [14] to account for the contribution of the liquid intermediate phase and for a conversion-dependent anisotropy ratio, $\xi = (1-\eta)\xi_b + \eta\xi_c$, which represents the progressive reduction of thermal anisotropy as the material transforms into char.

2.2. Model Implementation and Validation

The computational domain and boundary conditions are illustrated in **Figure 2**. Exploiting cylindrical symmetry, the model is solved over a two-dimensional axisymmetric quarter-domain defined by the axial coordinate $x \in [0, L/2]$ and the radial coordinate $r \in [0, R]$. The domain is discretized using a uniform finite difference grid, where the coupled mass and energy conservation equations are solved simultaneously at each time step. Time integration is performed using the

 doi:10.20944/preprints202604.1537.v1

MATLAB variable-step stiff solver (ode15s), with a maximum time step of 0.01 s. Symmetry boundary conditions are imposed at the central axis ($r = 0$) and the axial midplane ($x = 0$), while convective heat and mass transfer conditions are applied at the external boundaries ($x = L/2$ and $r = R$), where the particle exchanges heat and mass with the surrounding environment through the external heat transfer coefficient h.

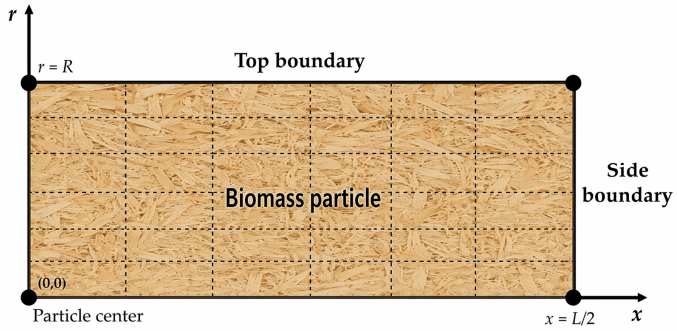

Figure 2. Diagram of the computational domain and mesh used for the numerical model of the biomass particle. The domain is defined in two-dimensional coordinates (x, r) exploiting the axial and radial symmetry axes.

Model predictions were validated against single-particle pyrolysis experiments for oak and birchwood at different reactor temperatures and heating rates, showing good agreement in both mass loss evolution and intraparticle temperature profiles [14].

2.3. Analysis Parameters

A parametric study was conducted to evaluate the influence of particle properties and operating conditions on biomass conversion, intraparticle liquid intermediate dynamics, and primary product yields during fast pyrolysis. The reference case corresponds to a cylindrical oak particle with a diameter of 3 mm and a length of 12 mm (aspect ratio 1:4), subjected to a reactor temperature of 500 °C and an external convective heat transfer coefficient of h = 359 $W \cdot m^{-2} \cdot K^{-1}$, with no initial moisture content. These conditions are consistent with the validation case reported by Sánchez et al. [14]. The lignocellulosic composition of oak was defined as 44% cellulose, 34% hemicellulose (GMSW softwood type), and 22% lignin (LIGH + LIGO).

2.3.1. Particle Size and Aspect Ratio

Particle size and geometry are key feedstock-specific parameters in fast pyrolysis, as they directly influence the surface-area-to-volume ratio and, consequently, the external heat transfer rate, as well as the development of intraparticle temperature and concentration gradients [6,20]. In cylindrical particles, the aspect ratio—defined as the length-to-diameter ratio—governs the relative importance of axial and radial heat transport during heating. Due to the pronounced anisotropy in the thermal conductivity and permeability of wood, particles with larger aspect ratios tend to develop stronger radial temperature gradients and exhibit longer conversion times compared to more equidimensional particles with the same diameter [10,14].

2.3.2. Initial Moisture Content

The initial moisture content of biomass is a critical process parameter, as raw feedstocks typically contain substantial amounts of water that must be removed prior to pyrolytic decomposition. Moisture evaporation is a strongly endothermic process that consumes heat during the early stages of pyrolysis, thereby reducing heating rates and postponing the onset of devolatilization reactions [22]. In the present model, moisture removal is represented using a lumped first-order expression that captures the combined effects of desorption, diffusion, and phase change [14].

 doi:10.20944/preprints202604.1537.v1

2.3.3. Lignocellulosic Composition

Biomass consists primarily of cellulose, hemicellulose, and lignin, which decompose through different pathways and at different rates, leading to distinct product distributions [22,23]. As a result, lignocellulosic composition strongly influences not only the yields of char, volatiles, gases, and water, but also the formation and evolution of liquid intermediates (metaplastic phase) within the particle. This phase plays a key role in intraparticle transport and intermediate residence times [24], and its bubbling behavior contributes to aerosol ejection, affecting the oligomeric and inorganic content of bio-oil [25–28]. To assess these effects, three feedstocks with contrasting compositions are considered: oak, sugarcane bagasse and palm shell, the latter characterized by a higher lignin content.

2.3.4. Reactor Temperature

Reactor temperature is a key operating parameter in fast pyrolysis, as it controls both the heating rate of the particle and the final temperature attained during conversion, thereby influencing products yields distribution. Elevated temperatures enhance devolatilization rates and tend to favor the formation of permanent gases at the expense of char and liquid products, whereas intermediate temperatures in the range of 450–550 °C are generally associated with maximum bio-oil yields [14,22,29].

2.3.5. Heating Rate

The heating rate of a biomass particle during fast pyrolysis is governed not only by reactor temperature but also by the external convective heat transfer coefficient, which is influenced by reactor design and gas flow conditions [3,30]. Higher heating rates promote volatile production over char, a behavior linked to the thermal and chemical evolution of the metaplastic phase within the particle [14,31]. In industrial systems such as fluidized beds, convective heat transfer coefficients can vary widely, from around 50 $W \cdot m^{-2} \cdot K^{-1}$ in poorly mixed regions to values above 1000 $W \cdot m^{-2} \cdot K^{-1}$ under highly fluidized conditions [12,30].

Table 2 summarizes the set of simulation cases considered in parametric analysis, including variations in particle properties and operating conditions.

Table 2. Summary of simulation cases for parametric analysis.

Parameter	Values studied	Fixed parameters
Particle size and aspect ratio	D×L: 3×3 mm (A.R. 1:1), 3×12 mm (A.R. 1:4), 8×8 mm (A.R. 1:1), 8×16 mm (A.R. 1:2), 8×24 mm (A.R. 1:3), and 8×32 mm (A.R. 1:4)	T = 500 °C, h = 359 $W \cdot m^{-2} \cdot K^{-1}$, oak, 0% moisture
Initial moisture content	0% and 12% (w/w)	D = 3 mm, L = 12 mm, T = 500 °C, h = 359 $W \cdot m^{-2} \cdot K^{-1}$, oak D = 8 mm, L = 32 mm, T = 500 °C, h = 359 $W \cdot m^{-2} \cdot K^{-1}$, oak
Lignocellulosic composition	Oak (CELL 44%, HCE 34%, LIG 22%), Sugarcane bagasse (CELL 28%, HCE 44%, LIG 23%, ashes 5%), Palm shell (CELL 27%, HCE 23%, LIG 50%)	D = 3 mm, L = 12 mm, T = 500 °C, h = 359 $W \cdot m^{-2} \cdot K^{-1}$, 0% moisture

 doi:10.20944/preprints202604.1537.v1

Heating rate (convective coefficient)	h = 50, 100, 150, 359, 1000, 1500 $W \cdot m^{-2} \cdot K^{-1}$	D = 3 mm, L = 12 mm, T = 500 °C, oak; 0% moisture
Reactor temperature	400, 500, 600, 700 °C	D = 3 mm, L = 12 mm, h = 359 $W \cdot m^{-2} \cdot K^{-1}$, oak, 0% moisture

3. Results and Discussion

3.1. Effect of Particle Size and Aspect Ratio

Figure 3 shows the effect of particle size and aspect ratio for oak particles with a convective coefficient of 359 W/m.K and reactor temperature of 500 °C; particles with diameters of 3mm and 8 mm and aspect ratios of 1:1 and 1:4 were modeled. As expected, smaller particles exhibit significantly smaller conversion times and char yields. Char yield was above 30% for larger particles in comparison with char yields around 20% for the smaller particles, and conversion time more than doubled for the large particles.

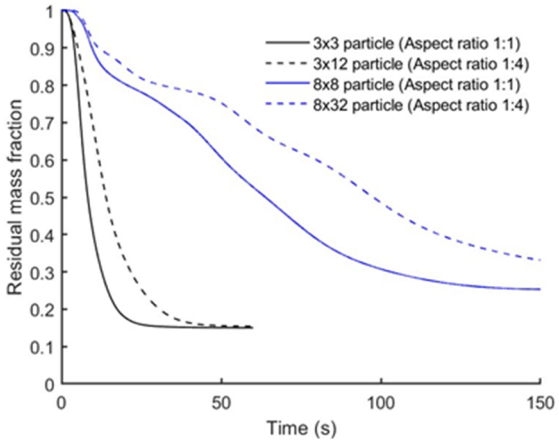

Figure 3. Effect of particle size and aspect ratio on particle conversion.

From a kinetic perspective, a smaller particle size during conversion can accelerate the local heating of the solid matrix, favoring primary devolatilization reactions and higher bio-oil yields. However, in larger particles, internal temperature gradients remain significant for longer periods, promoting heterogeneous reaction pathways associated with carbon formation and secondary reactions of volatile intermediates and hence exhibiting higher char yields. Particles with a higher aspect ratio exhibit steeper temperature gradients due to their elongated geometry, which increases the limitations of internal transport and delays temperature homogenization within the particle.

The Peclet number ($Pe = vR/\alpha$) compares convective and diffusive heat transport within the particle, and it can be used to analyze the effect of particle characteristics on transport phenomena within the particle. As shown in Figure 4, Pe increases sharply during the early stages, reaching a maximum that becomes higher as the aspect ratio (L/D) increases. This behavior indicates that heat transfer is predominantly advective, driven by the increase in internal gas velocity associated with devolatilization. As volatiles are generated, pressure builds within the particle, enhancing internal flow and thus increasing convective heat transport. Consequently, particles with larger L/D ratios exhibit higher peak Pe values due to greater resistance to gas escape, which intensifies pressure gradients and internal velocities. This trend is consistent with CFD studies reported by Kamila et al. [32], where internal convection driven by volatile release becomes more significant in larger particles and those with higher L/D ratios, affecting temperature fields and promoting non-uniform heating. After the peak, Pe gradually decreases, suggesting that the advective contribution weakens as volatile generation declines and internal pressures dissipate, leading the system back toward a conduction-influenced regime.

 doi:10.20944/preprints202604.1537.v1

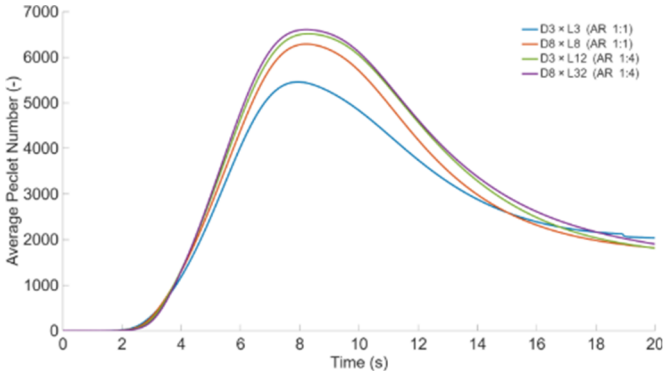

Figure 4. Average axial Peclet number as a function of time for biomass particles of different sizes and aspect ratios (D8–L8, D8–L16, D8–L24, D8–L32).

Furthermore, the pyrolysis transport map can be used to study the phenomena within the biomass particle and the effect of particle characteristics and process parameters in detail. Figure 5 shows that the conversion process for all four particle geometries is mainly located within the kinetically limited regime with noticeable inner temperature gradients ($Py_1 > 1$, Bi >1), however, as conversion progresses, the process evolves towards a transition regime were the limitation associated with heat transport begin to become relevant ($Py_1 > 1$, Bi between 0.1 and 10). This behavior highlights that, during the pyrolysis of cylindrical biomass particles, heat transfer, mass transport, and chemical kinetics can occur on comparable timescales, making it unsuitable to rely on simplified approaches that assume a single controlling resistance.

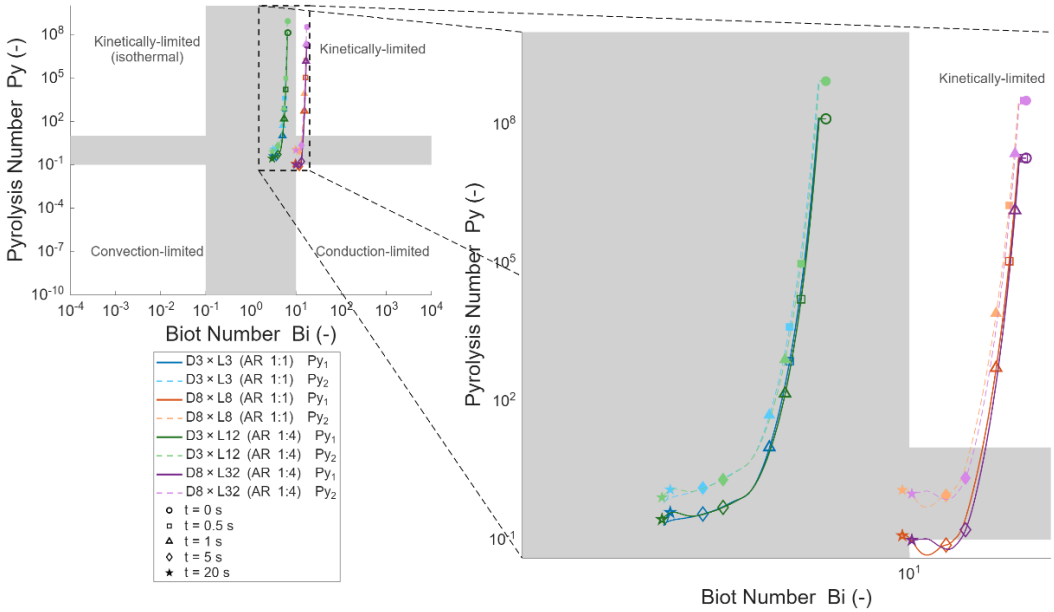

Figure 5. Pyrolysis transport map showing the temporal evolution of the dimensionless pyrolysis numbers Py_1 (solid lines) and Py_2 (dashed lines) as a function of the Biot number for four cylindrical biomass particle geometries with aspect ratios 1:1 and 1:4, under a fixed external heat transfer coefficient of h = 359 W m^{-2} K^{-1}. Markers indicate the particle state at selected conversion times (t = 0, 0.5, 1, 5, and 20 s).

Lumped-parameter models, which neglect internal temperature gradients (Bi ≪ 1), overpredict reaction rates by imposing isothermal conditions that are not representative of these particles, as evidenced by intraparticle simulations that report significant temperature heterogeneity for particles larger than 1 mm [33]. On the other hand, models that consider kinetics to be instantaneous relative to heat conduction fail to reproduce the early devolatilization stage observed between t = 0 and t = 1 s, where Py_1 decreases by several orders of magnitude as reaction rates increase exponentially with

 doi:10.20944/preprints202604.1537.v1

temperature—unlike the approximately linear temperature dependence assumed for effective thermal conductivity in this model. The particle aspect ratio (AR) also plays a relevant role: geometries with AR 1:4 consistently exhibit higher Py_1 values at early times compared to AR 1:1 particles of similar volume, in agreement with previous findings that higher aspect ratios enhance internal heat diffusion and accelerate mass loss [34]. Overall, these results support the conclusions of Pecha et al. [3], who showed that particles located in the transition regime of the pyrolysis transport map require models that simultaneously account for conduction, convection, and reaction kinetics.

3.2. Effect of the Initial Moisture Content

The effect of heat reactions of the moisture evaporation at the beginning of the process affects inner temperatures gradients and the particle mass loss rate. In ***Figure 6***a , which shows the evolution of the residual mass fraction (w/w) as a function of time, the particle with an initial moisture content of 12% exhibits a slower mass loss rate during the first few seconds of the process compared to the dry particle (0% moisture). This delay corresponds to the drying stage, where a significant portion of the supplied heat is consumed as latent heat of vaporization rather than contributing to the temperature increase or devolatilization. As a result, the onset of rapid mass loss is slightly delayed in the wet particle. However, once drying is complete, both curves converge and reach virtually the same final residual mass fraction and the same total conversion time (≈ 25–30 s). This indicates that moisture primarily affects the transient regime, rather than the final degree of conversion, under the same external heating conditions.

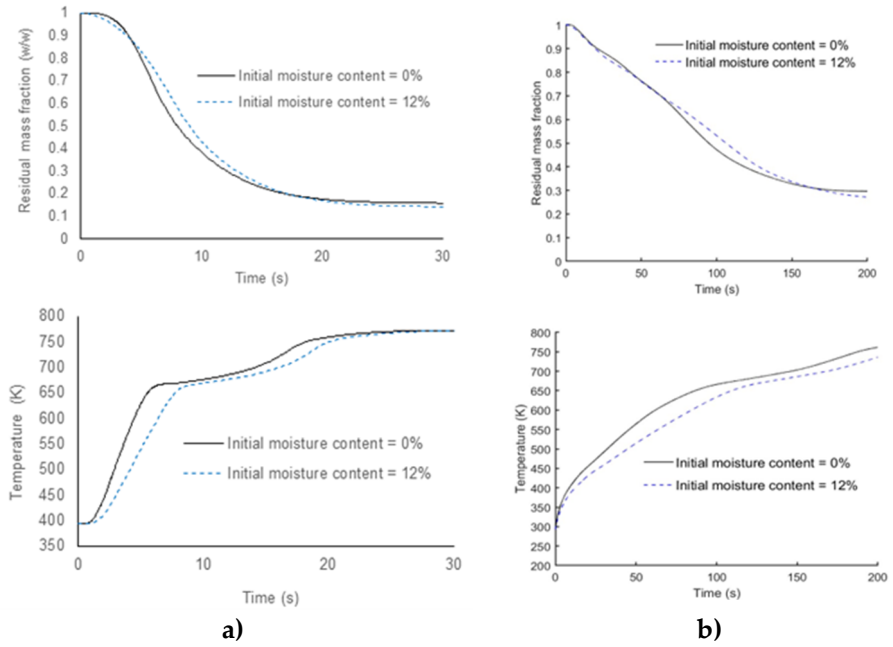

Figure 6. a) Effect of initial moisture content on mass loss evolution (top) and temperature profiles (bottom) (oak particle), T = 500 °C; h = 359 W·m^{-2}·K^{-1}, size = 3x12 mm. **b)** Effect of initial moisture content on mass loss evolution (top) and temperature profiles (bottom) (oak particle), T = 500 °C; h = 359 W·m^{-2}·K^{-1}, size = 8x32 mm.

This behavior is explained in more detail in Figure 6b, which shows the evolution of the particle's temperature. The particle with higher moisture content exhibits a slower temperature increase during the initial heating period around the boiling point of water, associated with evaporation. In contrast, the dry particle experiences a more pronounced temperature increase and reaches the devolatilization temperature range sooner. Consequently, higher internal temperature gradients are expected in the wet particle during the initial stage, as energy is redistributed between phase change and heat conduction toward the core.

These trends are consistent with previous findings reported in the literature. Studies on the pyrolysis of biomass particles have shown that higher initial moisture content delays devolatilization

 doi:10.20944/preprints202604.1537.v1

due to the additional energy required for water evaporation, without significantly altering the final charcoal yield under similar external heating conditions [35] This behavior is attributed to heat redistribution during the drying stage, which temporarily limits the temperature increase within the particle. Similarly, [36] analyzed the relationship between drying and pyrolysis and reported that moisture primarily affects the particle's temperature-time relationship, rather than altering the intrinsic kinetic parameters that govern devolatilization once the material is dry. Their results indicate that the main impact of moisture is a temporary shift in the onset of rapid mass loss.

Furthermore, numerical and thermochemical analyses, such as those discussed by [37] suggest that the differences between particles with varying moisture contents become more pronounced later during the drying stage, while the devolatilization phase proceeds in a comparable manner once similar internal temperatures are reached. Consequently, the overall product distribution is little affected by the initial moisture content under the current conditions, leading to comparable final carbon yields and volatile production despite the differences observed during the initial drying stage.

3.3. Effect of Lignocellulosic Composition on Product Yields and Liquid Intermediates Evolution

The lignocellulosic composition significantly influences the relative yields of charcoal and volatile products. Biomass with higher cellulose content and lower lignin content tends to produce greater quantities of volatile compounds and lower fractions of charcoal. This trend is observed in Figure 7, where the charcoal yields obtained for oak, sugarcane bagasse, and palm bark are 0.158, 0.208, 0.232, respectively, while the corresponding volatile yields are 0.588, 0.569, and 0.531. The higher volatile yield observed in cellulose-rich materials is associated with the thermal decomposition pathways of cellulose, which favor depolymerization and the formation of condensable volatile products. Conversely, lignin-rich raw materials generally produce higher charcoal yields due to their aromatic and highly cross-linked structure, which promotes carbonization reactions.

During fast pyrolysis of small particles, high heating rates throughout the particle are achieved, promoting rapid devolatilization reactions. Under these conditions, primary pyrolysis reactions predominate, favoring the formation and release of volatile products and limiting secondary carbon formation reactions within the particle.

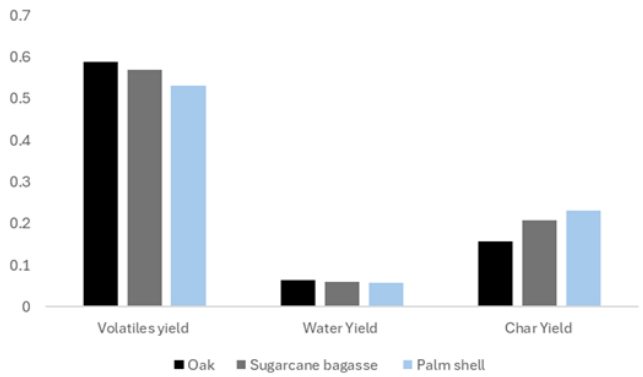

Figure 7. Effect of lignocellulosic composition on product yields.

Moreover, lignocellulosic composition not only affects the final yield of products such as char and volatiles but also affects the concentration of liquid intermediates within the particle as pyrolysis takes place. This is a relevant aspect since the appearance of the metaplast phase affects transport phenomena within the particle and the residence time of intermediate products [24]; additionally, the bubbling phenomenon within the metaplast phase causes the ejection of aerosols which contributes to the oligomers and inorganics content in bio-oil. This phenomenon is especially significant for fast

 doi:10.20944/preprints202604.1537.v1

pyrolysis where the concentrations of liquid intermediates within the particle are higher in comparison with pyrolysis at lower heating rates.

Pecha et al. [3] found that most of the liquid intermediates within the particle are derived from the lignin component; in Figure 8 the concentration of liquid intermediates for three different feedstocks are compared (oak, sugarcane bagasse and palm shell), it can be seen that concentration of the metaplast phase within the particle is significantly higher for palm shell (~35%) which have a higher concentration of lignin in comparison with oak husk.

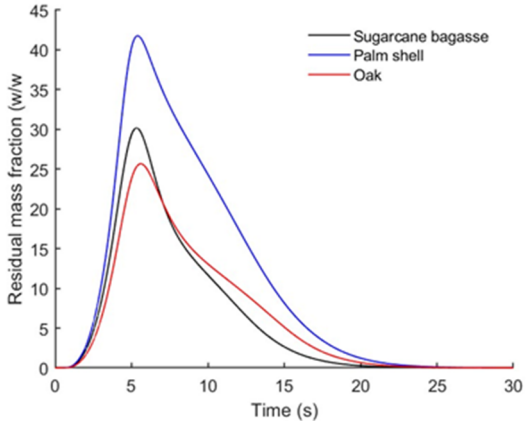

Figure 8. Effect of lignocellulosic composition on liquid intermediates concentration and evolution.

3.4. Effect of Heating Rate on Particle Mass Loss and Products Yields

Figure 9 shows the effect of the heating rate on the evolution of mass loss of an oak particle (D = 3 mm, L = 12 mm) at a reactor temperature of 500 °C. The heating rate was modified by varying the convective heat transfer coefficient from 50 to 1500 W m^{-2} K^{-1}. As shown in the figure, significant differences in the conversion rate were found under low heating conditions (h < 200 W m^{-2} K^{-1}). For lower convective coefficients, particle heating is controlled by external heat transfer, resulting in a slower temperature increase and longer conversion times.

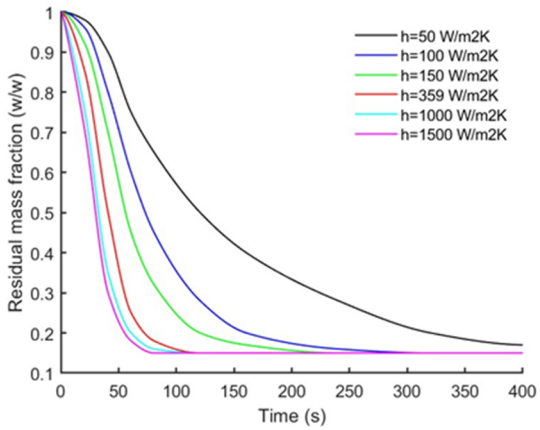

Figure 9. Effect of heating rate on particle mass loss (oak particle, D = 3 mm, L = 12 mm, T reactor = 500 °C).

As the heat transfer coefficient increases, the effect of heating rate on conversion time is less important. For heating conditions above approximately 1000 W m^{-2} K^{-1}, only small differences in the mass loss rate are observed, indicating that the overall process is increasingly controlled by intrinsic reaction kinetics. This trend is consistent with the widely reported behavior of biomass under rapid heating conditions, where a rapid temperature increase promotes primary devolatilization reactions

 doi:10.20944/preprints202604.1537.v1

and limits secondary carbon formation reactions within the particle. The increased volatile production at higher heating rates is attributed to the rapid generation and release of liquid-like intermediate species, which reduces the residence time of the secondary repolymerization reactions leading to carbon formation. These observations are consistent with previous studies on biomass pyrolysis kinetics and heat transfer phenomena, described by Várhegyi, Bridgwater and Michael J. Antal Jr., who highlighted the crucial role of heating rate in determining the competition between devolatilization and carbonization pathways during the thermochemical conversion of lignocellulosic materials [38–40].

The influence of the heating rate on product yields is shown in Figure 10. Higher heating rates promote the formation of volatile products. In the present results, an increase of approximately 2% in volatile yield is observed when the convective heat transfer coefficient increases from 50 to 1000 W m^{-2} K^{-1}. This behavior has been attributed to the rapid formation and accumulation of liquid-like intermediate species within the particle, which favors the release of condensable volatiles before secondary cracking or repolymerization reactions occur. Consequently, increasing the heating rate slightly reduces carbon and water production, while a moderate increase in permanent gas production is also observed. These trends are consistent with kinetic competition between the primary devolatilization reactions and the secondary carbon-forming reactions occurring within the particle.

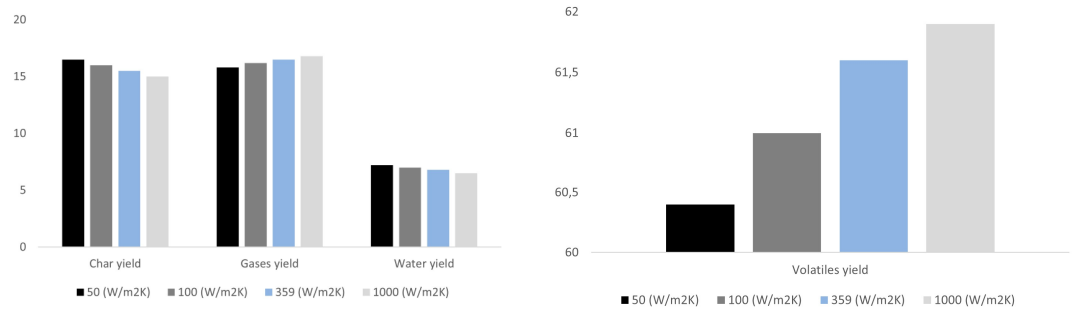

a) **b)**

Figure 10. Effect of heating rate on products yields (oak particle, D = 3 mm, L = 12 mm, Treactor = 500 °C). **a)** char, gases, and water yields; **b)** volatiles yield.) .

The pyrolysis transport map in Figure 11 shows that varying the external heat transfer coefficient from h = 50 to 1000 W m^{-2} K^{-1} produces a displacement of the process to higher Biot numbers where the relative importance of inner thermal conduction is higher and stronger temperature gradients within the particle can be found. Conversely, similar Py_1 can be found when the heating rate was changed, with most of the process being within the kinetically control regime, but with the relative importance of heat transfer resistance increasing as the conversion of the particle progress. At h = 50 W m^{-2} K^{-1}, representative of slow pyrolysis, the Biot number spans approximately 0.59 to 0.93, remaining consistently below unity and confirming that external convective resistance is the dominant thermal bottleneck with relatively modest intraparticle temperature gradients. At h = 100 W m^{-2} K^{-1}, the system begins at Bi ≈ 1.85 and decreases to Bi ≈ 0.97, placing it within a transitional regime where the controlling resistance shifts during the process. As h increases to 359 and 1000 W m^{-2} K^{-1}, representative of fast pyrolysis in fluidized bed reactors, the Biot number remains well above unity throughout the trajectory (Bi ≈ 3.3–6.6 and 8.2–18.5, respectively), indicating that internal conduction and chemical kinetics become simultaneously rate-controlling.

 doi:10.20944/preprints202604.1537.v1

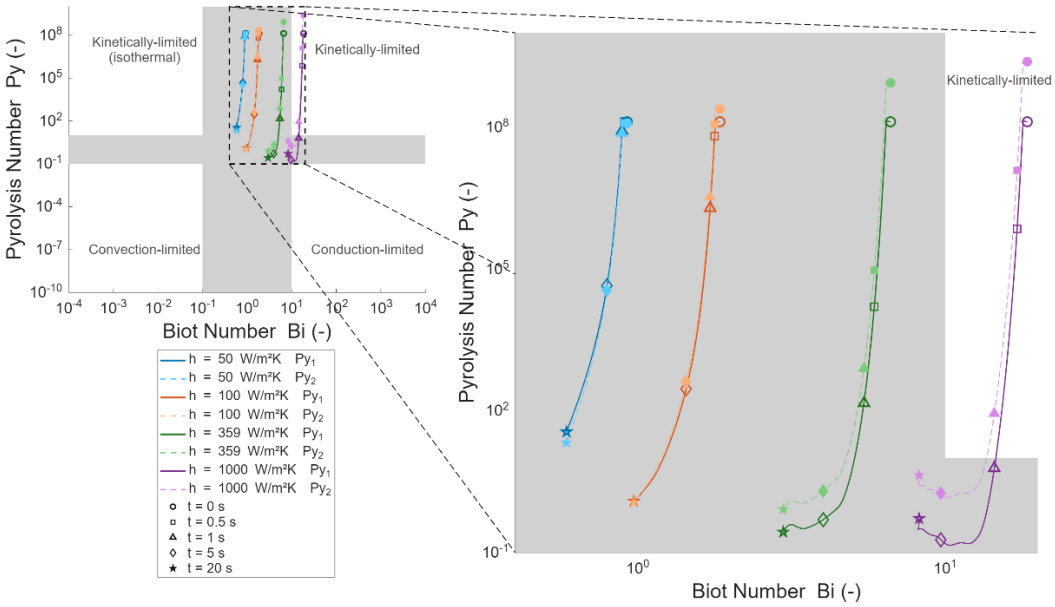

Figure 11. Pyrolysis transport map showing the temporal evolution of the dimensionless pyrolysis numbers Py_1 (solid lines) and Py_2 (dashed lines) as a function of the Biot number for a cylindrical biomass particle (D = 3 mm, L = 8 mm) subjected to external heat transfer coefficients ranging from h = 50 to h = 1000 W m^{-2} K^{-1}. Markers indicate the particle state at selected conversion times (t = 0, 0.5, 1, 5, and 20 s).

In the high-Biot-number regime, the exponential dependence of reaction rates on temperature implies that the steep internal gradients generated at high heating rates produce highly non-uniform devolatilization fronts that cannot be captured by lumped-parameter models, a limitation that becomes critical because kinetic rates vary exponentially with temperature while thermal conductivity varies only approximately linearly. Multi-fluid simulations of fluidized beds with thermally thick particles have confirmed that intraparticle temperature inhomogeneity under high heating rate conditions has a decisive influence on conversion predictions [41]. Furthermore, the Py_2 trajectories shift leftward with increasing h, confirming that higher heating rates compress the timescale over which kinetics and transport interact, consistent with the transport map framework established by Pecha et al [3], while multiscale simulations further demonstrate that neglecting particle-scale modeling leads to significant errors in predicted conversion profiles [42].

3.5. Effect of Reactor Temperature on Particle Mass Loss and Products Yields

The effects of reactor temperature on mass loss evolution are shown in Figure 12. As expected, the overall conversion time decreases significantly with increasing reactor temperature, since higher temperatures lead to higher heating rates and faster conversion kinetics of the biomass particle. For oak particles with a diameter of 3 mm and a length of 12 mm, the conversion time at reactor temperatures above 600 °C is below 20 s, whereas at temperatures around 400 °C the conversion process becomes considerably slower, exceeding 100 s, favoring the reaction route of char production, as it can be seen in Figure 13. This behavior is associated with the strong temperature dependence of the pyrolysis reaction kinetics, as the rates of thermal decomposition reactions increase exponentially with temperature.

 doi:10.20944/preprints202604.1537.v1

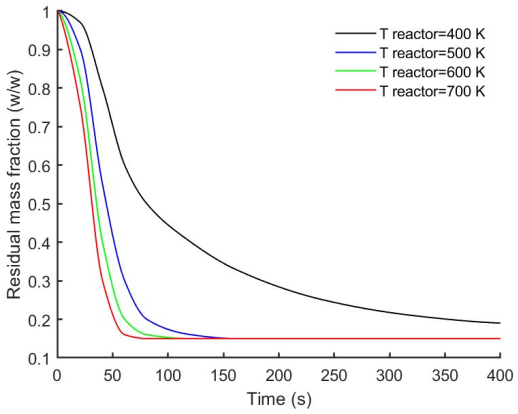

Figure 12. Effect of reactor temperature on particle mass loss (oak particle, D = 3 mm, L = 12 mm).

The influence of reactor temperature on the pyrolysis products yields is presented in Figure 13. At lower temperatures (under 500°C), the production of char notably increased. At higher reactor temperatures, high heating rates are promoted which in turn favor the production route of permanent gas and volatiles, however, an opposite effect also appears due to the charring reactions promoted at high temperatures. For the analyzed conditions, the net effect of these opposite effects resulted in an increase of permanent gases production, a reduction in char production and a less noticeable effect on the final yield of volatiles in the range from 500°C to 600°C. The maximum volatile yields are observed for reactor temperatures between 500 °C and 600 °C, which is consistent with previous studies on fast pyrolysis of lignocellulosic biomass. In this temperature range, the thermal decomposition of cellulose and hemicellulose favors depolymerization reactions that generate condensable volatile compounds.

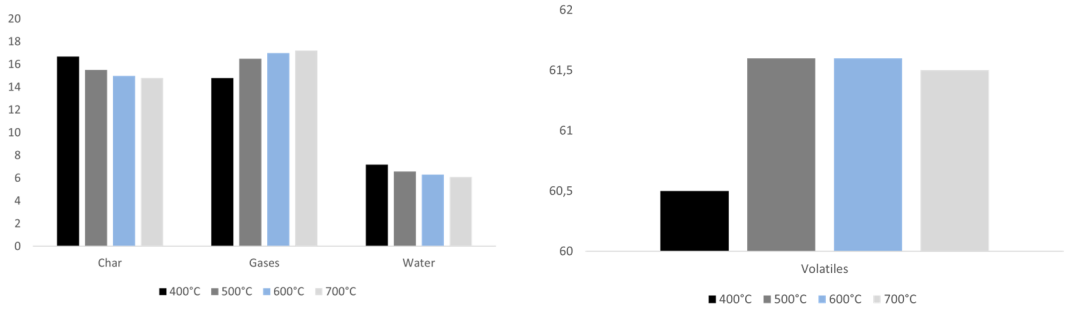

a) **b)**

Figure 13. Effect of reactor temperature on product yields (oak particle, D = 3 mm, L = 12 mm).

The comparison between the effects of reactor temperature and heating rate highlights two different thermochemical pathways governing biomass conversion. Increasing the heating rate generally promotes rapid devolatilization and favors the formation of volatile products such as bio-oil precursors, since the short residence time of intermediate species limits secondary reactions leading to char formation. In contrast, increasing the reactor temperature enhances secondary cracking and carbonization reactions, which can promote the formation of permanent gases and char at sufficiently high temperatures. Therefore, while the heating rate primarily controls the competition between primary devolatilization and char-forming reactions within the particle, the reactor temperature determines the extent of secondary charring reactions occurring during pyrolysis.

4. Conclusions

The parametric analysis conducted using the anisotropic single-particle model showed that particle size, aspect ratio, lignocellulosic composition, heating rate and reactor temperature

 doi:10.20944/preprints202604.1537.v1

significantly affect the conversion and products yields during fast pyrolysis of millimeter-scale biomass particles.

Dimensionless analysis through the Biot and Pyrolysis numbers confirms that cylindrical particles with diameters in the range of 3–8 mm operate in a regime, where internal conduction, external convection, and chemical kinetics act on comparable timescales. Larger particles and higher aspect ratios (AR 1:4) produce steeper radial temperature gradients, higher peak axial Peclet numbers, and longer conversion times, with internal convective transport driven by devolatilization-induced pressure gradients becoming increasingly significant as the length-to-diameter ratio increases. These results indicate that intraparticle transport anisotropy and particle geometry must be simultaneously accounted for in single-particle models to accurately predict both conversion times and product distributions.

The lignocellulosic composition of the particles significantly influences the relative yields of charcoal and volatile products. Biomass with higher cellulose content and lower lignin content tends to produce greater quantities of volatile compounds and lower fractions of charcoal. Furthermore, lignocellulosic composition also affected the formation and evolution of liquid intermediates (metaplastic phase) within the particle. The lignin fraction was found to be the dominant contributor to metaplast formation, and lignin-rich feedstocks such as palm shell exhibit significantly higher peak metaplast concentrations compared to cellulose-rich materials such as oak. This has direct implications for aerosol ejection phenomena in fast pyrolysis reactors, which affect the concentration of inorganic and heavy oligomeric compounds in bio-oil.

Heating rate and reactor temperature were found to significantly affect particle conversion kinetics. Increasing the convective heat transfer coefficient promotes rapid volatile release by accelerating metaplast formation and limiting secondary repolymerization reactions, yielding an increase of approximately 2% in volatile yield when h increases from 50 to 1000 $W \cdot m^{-2} \cdot K^{-1}$, while increasing reactor temperature enhances secondary cracking and permanent gas production, with maximum bio-oil yields observed in the 500–600 °C range.

The systematic parametric framework presented in this work, grounded in a physically consistent model with detailed CRECK kinetics and explicit tracking of intraparticle liquid intermediate evolution, provides a useful tool for reactor design and process optimization during the fast pyrolysis of biomass.

Author Contributions: Conceptualization, M.A.S., J.C.M.; Methodology, M.A.S.; Software, M.A.S., J.C.M., N.A.R.M. and F.L.; Validation, M.A.S., N.A.R.M. and F.L.; Formal analysis, M.A.S., J.C.M., N.A.R.M. and F.L.; Investigation, M.A.S., J.C.M., N.A.R.M. and F.L.; Resources, M.A.S.; Data curation, M.A.S., N.A.R.M. and F.L.; Writing—original draft preparation, M.A.S., N.A.R.M. and F.L.; Writing—review and editing, M.A.S., J.C.M., N.A.R.M. and F.L.; Visualization, M.A.S., N.A.R.M. and F.L.; Supervision, M.A.S. and J.C.M. All authors have read and agreed to the published version of the manuscript.

Funding: The authors want to thank the project "Modelamiento de la obtención de biochar mediante pirólisis de pellets de biomasa y evaluación experimental de su aplicación en la retención de contaminantes" code INV-CO-014-2022 by EIA University.

Data Availability Statement: The raw data supporting the conclusions of this article will be made available by the authors on request.

Acknowledgments: AI tools (ChatGTP 5.0) were used only for grammar and redaction aspects to shorten some of the paragraphs.

Conflicts of Interest: The authors declare no conflicts of interest.

Nomenclature

Symbol	Description	Units
b	biomass	-

 doi:10.20944/preprints202604.1537.v1

char	char	-
CELL	Cellulose	-
CELLA	Active cellulose	-
C_p	Particle local heat capacity	J·kg-1K-1
$C_{p,i}$	heat capacity of the gaseous components	J·kg-1K-1
D	Particle diameter	m
D_{eff_G}	Effective diffusivity of species in the gas phase	m2·s-1
G	Gas phase (permanent gases, volatiles, water vapor)	-
GAS	Permanent gases	-
h	External convective heat transfer coefficient	W·m-2·K-1
HCE	Hemicellulose	-
HCE1	Active hemicellulose type 1	-
HCE2	Active hemicellulose type 2	-
H_2O	Water vapor	-
H_{R_j}	Heat of reaction for reaction j	kJ·kg-1
i	Species or the reaction mechanism	-
j	Reactions of the reaction mechanism	-
$k_{m,i}$	External convective mass transfer coefficient	kg·s-1·m-2
K_G	Solid permeability to the gas mixture flow (axial direction)	m2
L	Particle length	m
L_0	Initial particle length	m
L_f	Final particle length	m
LIG-C	Carbon riched lignin	-
LIG-CC	Intermediate component from lignin	-
LIG-H	Hydrogen riched lignin	-
LIG-O	Oxygen riched lignin	-
LIG-OH	Intermediate component from lignin	-
LIG	Intermediate component from lignin	-
Nr	Total number of reactions	-
$\dot{N}_x''$	Mass flux in the axial direction	kg·m-2·s-1
P	Pressure of the gas mixture	Pa
$\dot{q}_x$	Heat flux in the axial direction	W·m-2
$\dot{q}_r$	Heat flux in the radial direction	W·m-2
r	Radial axis	m
$\dot{r}'''_{i,j}$	Reaction rate for the specie i in the reaction j	mol·m-3·s-1
R_0	Initial particle radius	m
R_f	Final particle radius	m
t	time	s-1
T	Temperature	K
T_∞	Temperature in the bulk phase	K
VOL.	Volatiles (light condensables)	-
v_G	Gas velocity	m·s-1

 doi:10.20944/preprints202604.1537.v1

x	Axial axis	m
Greek symbols		
ε_i	Component/phase fraction	-
$\bar{\eta}$	Average conversion of the particle	-
$\lambda_{eff,x}$	Effective conductivity in the axial direction	W·m-1·K-1
$\lambda_{eff,r}$	Effective conductivity in the radial direction	W·m-1·K-1
μ_g	Viscosity of the gas mixture	Pa·s
ξ	Relation between axial and radial effective thermal conductivity	-
ρ	Local particle density (estimated for each node)	kg·m-3
ρ_i^*	Mass concentration of the component i per particle volume	kg·m-3
$\rho_{i_g}^*$	Mass concentration of the component i in the gas phase per particle volume	kg·m-3
ρ_∞^*	Concentration of the specie i in the bulk phase	kg·m-3

References

1. M. S. Mettler, D. G. Vlachos, and P. J. Dauenhauer, "Top ten fundamental challenges of biomass pyrolysis for biofuels," *Energy Environ. Sci.*, vol. 5, no. 7, pp. 7797–7809, 2012, doi: 10.1039/C2EE21679E.
2. M. F. Crowley *et al.*, "Quantifying Impacts of Biomass Pelletization on Fast Pyrolysis Using a Single-Particle Reactor, X-ray Computed Tomography, and Computational Modeling," *Energy & Fuels*, vol. 40, no. 6, pp. 3136–3158, Feb. 2026, doi: 10.1021/acs.energyfuels.5c04362.
3. M. B. Pecha, J. I. M. Arbelaez, M. Garcia-Perez, F. Chejne, and P. N. Ciesielski, "Progress in understanding the four dominant intra-particle phenomena of lignocellulose pyrolysis: chemical reactions, heat transfer, mass transfer, and phase change," *Green Chem.*, vol. 21, no. 11, pp. 2868–2898, 2019, doi: 10.1039/C9GC00585D.
4. D. L. Pyle and C. A. Zaror, "Heat transfer and kinetics in the low temperature pyrolysis of solids," *Chem. Eng. Sci.*, vol. 39, no. 1, pp. 147–158, 1984, doi: https://doi.org/10.1016/0009-2509(84)80140-2.
5. A. Anca-Couce and N. Zobel, "Numerical analysis of a biomass pyrolysis particle model: Solution method optimized for the coupling to reactor models," *Fuel*, vol. 97, pp. 80–88, 2012, doi: 10.1016/j.fuel.2012.02.033.
6. H. Lu, E. Ip, J. Scott, P. Foster, M. Vickers, and L. L. Baxter, "Effects of particle shape and size on devolatilization of biomass particle," *Fuel*, vol. 89, no. 5, pp. 1156–1168, 2010, doi: 10.1016/j.fuel.2008.10.023.
7. X. Shi, F. Ronsse, and J. G. Pieters, "Finite element modeling of intraparticle heterogeneous tar conversion during pyrolysis of woody biomass particles," *Fuel Processing Technology*, vol. 148, pp. 302–316, 2016, doi: 10.1016/j.fuproc.2016.03.010.
8. G. Gentile, P. E. A. Debiagi, A. Cuoci, A. Frassoldati, E. Ranzi, and T. Faravelli, "A computational framework for the pyrolysis of anisotropic biomass particles," *Chemical Engineering Journal*, vol. 321, pp. 458–473, 2017, doi: 10.1016/j.cej.2017.03.113.
9. J. Blondeau and H. Jeanmart, "Biomass pyrolysis at high temperatures: Prediction of gaseous species yields from an anisotropic particle," *Biomass Bioenergy*, vol. 41, pp. 107–121, 2012, doi: 10.1016/j.biombioe.2012.02.016.
10. P. O. Okekunle, H. Watanabe, T. Pattanotai, and K. Okazaki, "Effect of biomass size and aspect ratio on intra-particle tar decomposition during wood cylinder pyrolysis," *Journal of Thermal Science and Technology*, vol. 7, no. 1, pp. 1–15, 2012, doi: 10.1299/jtst.7.1.
11. K. Kwiatkowski, B. Górecki, J. Korotko, W. Gryglas, M. Dudyński, and K. Bajer, "Numerical modeling of biomass pyrolysis - Heat and mass transport models," *Numeri. Heat Transf. A Appl.*, vol. 64, no. 3, pp. 216–234, 2013, doi: 10.1080/10407782.2013.779166.
12. B. Pecha *et al.*, "Integrated Particle- and Reactor-Scale Simulation of Pine Pyrolysis in a Fluidized Bed," *Energy and Fuels*, vol. 32, no. 10, pp. 10683–10694, 2018, doi: 10.1021/acs.energyfuels.8b02309.
13. C. Di Blasi, "Physico-chemical processes occurring inside a degrading two-dimensional anisotropic porous medium," *Int. J. Heat Mass Transf.*, vol. 41, no. 24, pp. 4139–4150, 1998, doi: 10.1016/S0017-9310(98)00142-2.

 doi:10.20944/preprints202604.1537.v1

14. M. Sánchez, J. C. Maya, B. Pecha, F. Chejne, and A. M. Quinchía-Figueroa, "Effect of particle characteristics, kinetics and transport phenomena on the prediction of particle mass loss and products yields during biomass fast pyrolysis," *J. Anal. Appl. Pyrolysis*, vol. 168, p. 105786, 2022, doi: https://doi.org/10.1016/j.jaap.2022.105786.
15. P. Debiagi, G. Gentile, A. Cuoci, A. Frassoldati, E. Ranzi, and T. Faravelli, "A predictive model of biochar formation and characterization," *J. Anal. Appl. Pyrolysis*, vol. 134, no. June, pp. 326–335, 2018, doi: 10.1016/j.jaap.2018.06.022.
16. S. Maduskar, G. G. Facas, C. Papageorgiou, C. L. Williams, and P. J. Dauenhauer, "Five Rules for Measuring Biomass Pyrolysis Rates: Pulse-Heated Analysis of Solid Reaction Kinetics of Lignocellulosic Biomass," *ACS Sustain. Chem. Eng.*, vol. 6, no. 1, pp. 1387–1399, Jan. 2018, doi: 10.1021/acssuschemeng.7b03785.
17. L. Lu *et al.*, "Investigating biomass composition and size effects on fast pyrolysis using global sensitivity analysis and CFD simulations," *Chemical Engineering Journal*, vol. 421, p. 127789, 2021, doi: https://doi.org/10.1016/j.cej.2020.127789.
18. T. Lihra, A. Cloutier, and S.-Y. Zhang, "Longitudinal and transverse permeability of balsam fir wetwood and normal heartwood," *Wood and Fiber Science*, vol. 32, no. 2, pp. 164 – 178, 2000, [Online]. Available: https://www.scopus.com/inward/record.uri?eid=2-s2.0-0041036536&partnerID=40&md5=19c177f01699b9eb39cb8c3f6c9c375b
19. F. F. P. Kollmann, E. W. Kuenzi, and A. J. Stamm, "Principles of Wood Science and Technology," *Principles of Wood Science and Technology*, 1968, doi: 10.1007/978-3-642-87931-9.
20. P. N. Ciesielski *et al.*, "Biomass Particle Models with Realistic Morphology and Resolved Microstructure for Simulations of Intraparticle Transport Phenomena," *Energy & Fuels*, vol. 29, no. 1, pp. 242–254, Jan. 2015, doi: 10.1021/ef502204v.
21. M. Bellais, K. O. Davidsson, T. Liliedahl, K. Sjöström, and J. B. C. Pettersson, "Pyrolysis of large wood particles: A study of shrinkage importance in simulations," *Fuel*, vol. 82, no. 12, pp. 1541–1548, 2003, doi: 10.1016/S0016-2361(03)00062-0.
22. C. Di Blasi, "Modeling chemical and physical processes of wood and biomass pyrolysis," *Prog. Energy Combust. Sci.*, vol. 34, no. 1, pp. 47–90, 2008, doi: 10.1016/j.pecs.2006.12.001.
23. M. G. Grønli, G. Várhegyi, and C. Di Blasi, "Thermogravimetric analysis and devolatilization kinetics of wood," *Ind. Eng. Chem. Res.*, vol. 41, no. 17, pp. 4201 – 4208, 2002, doi: 10.1021/ie0201157.
24. A. Dufour, B. Ouartassi, R. Bounaceur, and A. Zoulalian, "Modelling intra-particle phenomena of biomass pyrolysis," *Chemical Engineering Research and Design*, vol. 89, no. 10, pp. 2136–2146, 2011, doi: 10.1016/j.cherd.2011.01.005.
25. J. Montoya, B. Pecha, F. C. Janna, and M. Garcia-Perez, "Micro-explosion of liquid intermediates during the fast pyrolysis of sucrose and organosolv lignin," *J. Anal. Appl. Pyrolysis*, vol. 122, pp. 106–121, 2016, doi: https://doi.org/10.1016/j.jaap.2016.10.010.
26. S. Zhou, B. Pecha, M. van Kuppevelt, A. G. McDonald, and M. Garcia-Perez, "Slow and fast pyrolysis of Douglas-fir lignin: Importance of liquid-intermediate formation on the distribution of products," *Biomass Bioenergy*, vol. 66, pp. 398–409, 2014, doi: https://doi.org/10.1016/j.biombioe.2014.03.064.
27. A. R. Teixeira *et al.*, "Aerosol generation by reactive boiling ejection of molten cellulose," *Energy Environ. Sci.*, vol. 4, no. 10, pp. 4306–4321, 2011, doi: 10.1039/c1ee01876k.
28. N. Jendoubi, F. Broust, J. M. Commandre, G. Mauviel, M. Sardin, and J. Lédé, "Inorganics distribution in bio oils and char produced by biomass fast pyrolysis: The key role of aerosols," *J. Anal. Appl. Pyrolysis*, vol. 92, no. 1, pp. 59–67, 2011, doi: 10.1016/j.jaap.2011.04.007.
29. P. O. Okekunle, T. Pattanotai, H. Watanabe, and K. Okazaki, "Numerical and experimental investigation of intra-particle heat transfer and tar decomposition during pyrolysis of wood biomass," *Journal of Thermal Science and Technology*, vol. 6, no. 3, pp. 360–375, 2011.
30. M. B. Pecha *et al.*, "Impacts of Anisotropic Porosity on Heat Transfer and Off-Gassing during Biomass Pyrolysis," *Energy & Fuels*, vol. 35, no. 24, pp. 20131–20141, Dec. 2021, doi: 10.1021/acs.energyfuels.1c02679.
31. J. Montoya, B. Pecha, F. Chejne, and M. Garcia-Perez, "Single particle model for biomass pyrolysis with bubble formation dynamics inside the liquid intermediate and its contribution to aerosol formation by thermal ejection," *J. Anal. Appl. Pyrolysis*, vol. 124, pp. 204–218, 2017, doi: 10.1016/j.jaap.2017.02.004.

 doi:10.20944/preprints202604.1537.v1

32. B. Kamila, A. K. Sadhukhan, and P. Gupta, "2D CFD modeling for pyrolysis of a large biomass particle: Effect of L/D ratio, internal convection and shrinkage," *Chemical Engineering Research and Design*, vol. 208, pp. 921–933, 2024, doi: https://doi.org/10.1016/j.cherd.2024.07.002.
33. H. Fatehi, W. Weng, Z. Li, X. S. Bai, and M. Aldén, "Recent development in numerical simulations and experimental studies of biomass thermochemical conversion," May 06, 2021, *American Chemical Society*. doi: 10.1021/acs.energyfuels.0c04139.
34. J. Wang, X. Ku, and Z. Liu, "Three-Dimensional Simulation of the Pyrolysis of a Thermally Thick Biomass Particle," *Energy & Fuels*, vol. 37, no. 6, pp. 4413–4428, Mar. 2023, doi: 10.1021/acs.energyfuels.2c03675.
35. Y. Wu *et al.*, "Effect of biomass components' interaction on the pyrolysis reaction kinetics and small-molecule product release characteristics," *J. Anal. Appl. Pyrolysis*, vol. 173, p. 106039, Aug. 2023, doi: 10.1016/j.jaap.2023.106039.
36. M. Müller-Hagedorn and H. Bockhorn, "Pyrolytic behaviour of different biomasses (angiosperms) (maize plants, straws, and wood) in low temperature pyrolysis," *J. Anal. Appl. Pyrolysis*, vol. 79, no. 1–2, pp. 136–146, May 2007, doi: 10.1016/j.jaap.2006.12.008.
37. E. Ranzi, P. E. A. Debiagi, and A. Frassoldati, "Mathematical Modeling of Fast Biomass Pyrolysis and Bio-Oil Formation. Note II: Secondary Gas-Phase Reactions and Bio-Oil Formation," *ACS Sustain. Chem. Eng.*, vol. 5, no. 4, pp. 2882–2896, Apr. 2017, doi: 10.1021/acssuschemeng.6b03098.
38. A. V. Bridgwater, "Review of fast pyrolysis of biomass and product upgrading," *Biomass Bioenergy*, vol. 38, pp. 68–94, Mar. 2012, doi: 10.1016/j.biombioe.2011.01.048.
39. G. Várhegyi, B. Bobály, E. Jakab, and H. Chen, "Thermogravimetric Study of Biomass Pyrolysis Kinetics. A Distributed Activation Energy Model with Prediction Tests," *Energy & Fuels*, vol. 25, no. 1, pp. 24–32, Jan. 2011, doi: 10.1021/ef101079r.
40. M. J. Antal and M. Grønli, "The Art, Science, and Technology of Charcoal Production," *Ind. Eng. Chem. Res.*, vol. 42, no. 8, pp. 1619–1640, Apr. 2003, doi: 10.1021/ie0207919.
41. H. Luo *et al.*, "Multi-fluid modeling of heat transfer in bubbling fluidized bed with thermally-thick particles featuring intra-particle temperature inhomogeneity," *Chemical Engineering Journal*, vol. 460, Mar. 2023, doi: 10.1016/j.cej.2023.141813.
42. X. Gao, J. Yu, L. Lu, and W. A. Rogers, "Coupling particle scale model and SuperDEM-CFD for multiscale simulation of biomass pyrolysis in a packed bed pyrolyzer," *AIChE Journal*, vol. 67, no. 4, p. e17139, 2021, doi: https://doi.org/10.1002/aic.17139.